Chemical Physics Letters 496 (2010) 188–195

Contents lists available at ScienceDirect

Chemical Physics Letters

journal homepage: www.elsevier.com/locate/cplett

Time-dependent density-functional theory method in the electron nuclear dynamics framework

S. Ajith Perera [a,b], Patrick M. McLaurin [a], Thomas V. Grimes [a], Jorge A. Morales [a,*]

[a] Department of Chemistry and Biochemistry, Texas Tech University, P.O. Box 41061, Lubbock, TX 79409-1061, USA
[b] Department of Chemistry, Quantum Theory Project, University of Florida, Gainesville, FL 32611, USA

ARTICLE INFO

Article history:
Received 12 May 2010
In final form 12 July 2010
Available online 15 July 2010

ABSTRACT

A time-dependent density-functional theory (DFT) dynamics method in the electron nuclear dynamics (END) framework is presented. This time-dependent variational method treats simultaneously the nuclei and electrons of a system without utilizing predetermined potential energy surfaces. Like the simplest-level END, this method adopts a classical-mechanics description for the nuclei and a Thouless single-determinantal representation for the electrons. However, the electronic description is now expressed in a Kohn–Sham DFT form that provides electron correlation effects absent in the simplest-level END. Current implementation of this method employs the adiabatic approximation in the exchange–correlation action and potential. Simulations of molecular vibrations and proton–molecule reactions attest to the accuracy of the present method.

1. Introduction

The electron nuclear dynamics (END) [1–3] theory of Deumens and Öhrn is a time-dependent, variational, nonadiabatic method that treats simultaneously the nuclei and electrons of a molecular system. As a direct-dynamics method [4–8], END calculates the forces acting among the reaction participants '*on the fly*', *i.e.*, as the reaction simulation proceeds. That calculation scheme eludes the arduous predetermination of complete potential energy surfaces, as is the case for more traditional approaches. In that framework, END prescribes a total trial wavefunction $|\Psi_{END}\rangle$ for both the nuclei and the electrons. The END dynamical equations are obtained by applying the time-dependent variational principle (TDVP) [9] to $|\Psi_{END}\rangle$ in terms of the quantum action and Lagrangian A_{END} and L_{END}, respectively,

$$A_{END}\left[\Psi^*_{END},\Psi_{END}\right]=\int_{t_1}^{t_2} dtL_{END}\left[\Psi^*_{END},\Psi_{END}\right]$$
$$L_{END}\left[\Psi^*_{END},\Psi_{END}\right]=\langle\Psi_{END}|i\frac{\partial}{\partial t}-\widehat{H}_{Total}|\Psi_{END}\rangle\langle\Psi_{END}|\Psi_{END}\rangle^{-1} \quad (1)$$

where $\widehat{H}_{Total}$ is the total Hamiltonian. The END dynamical equations are obtained by imposing the stationary condition to A_{END}, $\delta A_{END}\left[\Psi^*_{END},\Psi_{END}\right]=\delta\int_{t_1}^{t_2} dtL_{END}\left[\Psi^*_{END},\Psi_{END}\right]=0$, with boundary conditions $\delta|\Psi_{END}\ (t_1)\rangle=\delta|\Psi_{END}\ (t_2)\rangle=0$. That stationary condition leads to a set of Euler–Lagrange equations for the variational parameters of $|\ \Psi_{END}\rangle$ that determine its time evolution. Within the above characterization, END adopts various levels of realizations according to the nuclear and the electronic descriptions imparted on $|\Psi_{END}\rangle$. The simplest-level END (SLEND) [1–3] adopts a trial total wavefunction $|\Psi_{SLEND}\rangle=|\Psi_N\rangle|\Psi_e\rangle$, where the nuclear wavefunction $|\Psi_N\rangle$ is a product of frozen, narrow-width Gaussian wave packets, and the electronic wavefunction $|\Psi_e\rangle$ is a Thouless single-determinantal state [10]. In practice, $|\Psi_N\rangle$ is used in the limit of zero wave-packet widths that provides a classical-mechanics description for the nuclei. Due to suitable parameterizations in $|\Psi_N\rangle$ and $|\Psi_e\rangle$, the SLEND dynamical equations exhibit a generalized symplectic form [9] that closely resembles the classical Hamilton equations [11]. SLEND is the most utilized version of END and has proven accurate for the simulation of proton–molecule ($H^+ + M$, $M = H_2$ [12,13], CH_4 [14], H_2O[15], C_2H_2 [16,17], HF[18], CF_4 [19], *etc.*), hydrogen–molecule ($H + D_2$ [20], H + HOD [21], *etc.*), and molecule–molecule ($D_2 + NH_3^+$ [22], *etc.*) reactions, *inter alia.*

Despite the SLEND suitability to describe the aforesaid systems, the study of more complex reactions will require higher-level END realizations featuring more elaborated descriptions for the nuclei and electrons [3]. For instance, for nuclei, the simulation of classically-forbidden phenomena (*e.g.* tunneling) will require quantum treatments. END can generate a quantum nuclear description of its own type [3] by employing nuclear wavefunctions involving nuclear molecular orbitals (*cf.* Ref. [23,24]). However, that extension will not be considered here, and the SLEND nuclear classical mechanics—appropriate to simulate the aforesaid type of systems—will be retained. (Nonetheless, see Refs. [12,13,25] about the reconstruction of quantum probabilities for rotational and vibrational excitations from the SLEND nuclear classical dynamics using coherent states [26]; conversely, see Ref. [27] about

* Corresponding author. Fax: +1 806 742 1289.
E-mail address: jorge.morales@ttu.edu (J.A. Morales).

0009-2614/$ - see front matter © 2010 Elsevier B.V. All rights reserved.
doi:10.1016/j.cplett.2010.07.034

obtaining classical-electrostatics models for the electrons from quantum valence-bond states). For electrons, a more needed improvement in SLEND is the inclusion of electron correlation. One way to achieve that is to go beyond a single-determinantal representation and incorporate post-Hartree–Fock methods [28] into the END framework (*e.g.* multi-configurational [29] or coupled-cluster [30] methods), but the resulting dynamical equations will be computationally expensive. Alternatively, a more feasible approach is to retain the SLEND single-determinantal representation and include electron correlation via the time-dependent (TD) Kohn–Sham (KS) density-functional theory (DFT: TDKSDFT) [31–34]. That approach leads to the new END/KSDFT method introduced here.

The END/KSDFT formulation takes advantage of two similarities between SLEND and TDKSDFT: both theories employ electronic single-determinantal states and admit equivalent TDVP formulations [1–3,31–34]. While those aspects have been discussed for SLEND, a concise review of the analogous aspects of TDKSDFT is necessary to elucidate the END/KSDFT formulation.

TDKSDFT has its foundation in the Runge–Gross theorem [31]. That theorem affirms that there is a one-to-one correspondence between the time-dependent external potential $v_{ext}(\mathbf{r},t)$ and the electron density $\rho(\mathbf{r},t)$ of a time-evolving system. That one-to-one mapping implies that the time-dependent electron density $\rho(\mathbf{r},t)$ completely determines the time-dependent wavefunction $|\Psi[\rho](t)\rangle$ and properties of a system. In that framework, the search of the exact electron density $\rho(\mathbf{r},t)$ admits a TDVP formulation through the quantum action $A[\rho]$ [31–34]

$$A[\rho] = \int_{t_1}^{t_2} dt \left\langle \Psi[\rho](t) \left| i\frac{\partial}{\partial t} - \widehat{H}(t) \right| \Psi[\rho](t) \right\rangle \tag{2}$$

Unlike A_{END}, Eq. (1), $A[\rho]$ usually involves a normalized trial wavefunction $|\Psi[\rho](t)\rangle$ [31–34]; however, both types of actions are equivalent under TDVP treatments [9]. The exact electron density $\rho(\mathbf{r},t)$ corresponds to the TDVP stationary condition $\delta A[\rho]/\delta\rho(\mathbf{r},t) = 0$, with boundary conditions $\delta|\Psi[\rho](t_1)\rangle = \delta|\Psi[\rho](t_2)\rangle = 0$ [31–33]. A practical way to obtain $\rho(\mathbf{r},t)$ from that stationary condition implies casting $A[\rho]$ into the KS form [31–33,35]. That approach invokes an auxiliary system of N_e non-interacting electrons described by the KS single-determinantal wavefunction $\Phi(\mathbf{r}_1,\ldots,\mathbf{r}_{N_e},t) = \det[\psi_i(\mathbf{r}_i,t)]/\sqrt{N_e!}$ involving orthonormal KS spin–orbitals $\{\psi_i(\mathbf{r}_i,t)\}$. The auxiliary system is subject to an effective external potential $v_s[\rho](\mathbf{r},t)$ (unique by the Runge–Gross theorem) so that its electron density $\rho(\mathbf{r},t) = \sum_{i=1}^{N_e}|\psi_i(\mathbf{r}_i,t)|^2$ is assumed to be identical to the electron density of the actual system of N_e interacting electrons. Then, the actual system action $A[\rho]$ can be expressed as [31–33]

$$\begin{aligned} A[\rho] = {} & \int_{t_1}^{t_2} dt \left\langle \Phi[\rho](t) \left| i\frac{\partial}{\partial t} - \widehat{T}_e \right| \Phi[\rho](t) \right\rangle - \int_{t_1}^{t_2} dt \\ & \times \int d\mathbf{r}\rho(\mathbf{r},t)\, v_{ext}(\mathbf{r},t) - \frac{1}{2}\int_{t_1}^{t_2} dt \int\int d\mathbf{r}d\mathbf{r}' \\ & \times \frac{\rho(\mathbf{r},t)\rho(\mathbf{r}',t)}{|\mathbf{r}-\mathbf{r}'|} - A_{xc}[\rho] \end{aligned} \tag{3}$$

where $|\Phi[\rho](t)\rangle$ is the KS single-determinantal wavefunction, $\widehat{T}_e$ the electronic kinetic energy operator, and $A_{xc}[\rho]$ the exchange–correlation part of $A[\rho]$. Application of the TDVP to $A[\rho]$ of Eq. (3) and to its analogue for the auxiliary non-interacting system renders an expression for $v_s[\rho](\mathbf{r},t)$

$$\begin{aligned} & v_s[\rho](\mathbf{r},t) = v_{ext}(\mathbf{r},t) + \int \frac{d\mathbf{r}'\rho(\mathbf{r}',t)}{|\mathbf{r}-\mathbf{r}'|} + v_{xc}[\rho](\mathbf{r},t); \\ & v_{xc}[\rho](\mathbf{r},t) = \frac{\delta A_{xc}[\rho]}{\delta\rho(\mathbf{r},t)} \end{aligned} \tag{4}$$

where $v_{ext}(\mathbf{r},t)$ is the external potential on the actual system, $\int d\mathbf{r}'\rho(\mathbf{r}',t)/|\mathbf{r}-\mathbf{r}\prime|$ the electronic repulsion potential, and $v_{xc}[\rho](\mathbf{r},t)$ the exchange–correlation potential [31–33]. The time evolution of $\rho(\mathbf{r},t)$ is determined by the time evolution of the KS spin–orbitals, each of them obeying a time-dependent Schrödinger equation having the potential $v_s[\rho](\mathbf{r},t)$ [31–33]. Clearly, the TDVP-formulated TDKSDFT, complemented with a classical treatment for the moving nuclei, can be incorporated into the SLEND framework to generate the END/KSDFT method. In fact, Theilhaber [36] developed a direct-dynamics method from the above TDKSDFT action that included a classical treatment for the moving nuclei. Although not in the END framework, Theilhaber's method certainly inspired the present END/KSDFT.

Further progress in any TDKSDFT effort depends upon obtaining an expression for $A_{xc}[\rho]$ (or $v_{xc}[\rho](\mathbf{r},t)$): a term unknown in its exact form, but for which various approximations have been proposed [32–34]. The simplest and most widespread approximation to $A_{xc}[\rho]$ is the adiabatic approximation [32–34]:

$$\begin{aligned} A_{xc}[\rho] \approx A_{xc}^{adia.}[\rho] = \int_{t_1}^{t_2} dt E_{xc}^{gs}[\rho]; \quad v_{xc}^{adia.}[\rho](\mathbf{r},t) = \frac{\delta A_{xc}^{adia.}[\rho]}{\delta\rho(\mathbf{r},t)} \\ = v_{xc}^{gs}[\bar{\rho}](\mathbf{r})\big|_{\bar{\rho}(\mathbf{r})=\rho(\mathbf{r},t)} \end{aligned} \tag{5}$$

where $E_{xc}^{gs}[\rho]$ and $v_{xc}^{gs}[\bar{\rho}](\mathbf{r})$ are ground-state, time-independent KSDFT, exchange–correlation energy functionals and potentials, respectively. The adiabatic approximation is extensively used in linear-response TDKSDFT calculations of excitation energies [32–34] and also in Theilhaber's direct-dynamics method [36], in both cases producing satisfactory results. The adiabatic approximation should work well with slow-evolving electron densities that remain near the ground state; however, previous TDKSDFT experience [33,34] suggests that this approximation can work acceptably even with processes beyond the slow and near-ground-state regime, as is the case for some chemical reactions. For all those reasons (and for another one discussed shortly), the adiabatic approximation is adopted in the present END/KSDFT implementation. More accurate approximations to A_{xc} [ρ] [32–34] will be tried in the future.

An additional motivation to adopt the adiabatic approximation is its *ad hoc* solution to two interrelated problems found in the TDVP-formulated TDKSDFT [33,34]. The first of those problems, the '*causality paradox*', is that action-derived exchange–correlation kernels $f_{xc}[\rho](\mathbf{r},t,\ \mathbf{r}',t') = \delta v_{xc}[\rho](\mathbf{r},t)/\delta\rho(\mathbf{r}',t') = \delta^2 A_{xc}[\rho]/\delta\rho(\mathbf{r},t)\,\delta\rho(\mathbf{r}',t')$ do not satisfy the necessary causality condition $f_{xc}[\rho](\mathbf{r},t,\mathbf{r}',t') = 0$ for $t' > t$ in most cases. The second problem is that in the context of the Runge–Gross theorem, the initial boundary condition $\delta|\Psi[\rho](t_1)\rangle = 0$ completely determines the final variation $\delta|\Psi[\rho](t_2)\rangle$; therefore, it is no longer possible to set the final TDVP boundary condition $\delta|\Psi[\rho](t_2)\rangle = 0$ independently [34,37,38]. The two problems have motivated several sophisticated solutions to correct the TDVP-formulated TDKSDFT [37–40]. However, it is unclear if those sophisticated solutions can be implemented into a computationally feasible method like END/KSDFT. More recently, Vignale [41] demonstrated that the two problems can be solved if the TDVP stationary condition $\delta A[\rho] = 0$ with the two boundary conditions is substituted for the condition $\delta A[\rho] = i\langle\Psi[\rho](t_2)|\delta\Psi[\rho](t_2)\rangle$—where the latter term is the non-zero final-endpoint variation—with one boundary condition at the initial endpoint $\delta|\Psi[\rho](t_1)\rangle = 0$. This modified variational principle leads to the exchange–correlation potential $v_{xc}[\rho](\mathbf{r},t)$ of Eq. (4), but with additional terms from the non-zero final-endpoint variation that restores causality to $f_{xc}[\rho]$ $(\mathbf{r},t,\ \mathbf{r}',t')$. Vignale's solution involving the traditional quantum action in real time is amenable to formulate a problem-free END/KSDFT, which is under consideration in our group. Until that rigorous END/KSDFT becomes available, we can safely restore causality within the standard TDVP by adopting the adiabatic approximation (*cf.* Ref. [33,34]) since $f_{xc}^{adia.}[\rho](\mathbf{r},t,\mathbf{r}',$

$t') = \delta v_{xc}^{adia.}[\rho](\mathbf{r},t)/\delta\rho(\mathbf{r}',t') = \delta(t-t')\delta v_{xc}^{gs}[\tilde{\rho}](\mathbf{r})/\delta\tilde{\rho}(\mathbf{r}')\big|_{\tilde{\rho}(\mathbf{r})=\rho(\mathbf{r},t)}$: an expression local in time and therefore causal. With causality so repaired, Vignale's causality-restoring final-endpoint variation becomes somewhat superfluous and can be neglected; thus, the standard TDVP stationary condition $\delta A[\rho] = 0$ with two boundary conditions is recovered. Notice that the standard TDVP with the adiabatic approximation was also employed in Theilhaber's direct-dynamical method [36], where it produced physically sound results.

Having reviewed END and TDKSDFT, the END/KSDFT method is now presented. A forerunner of END/KSDFT was introduced by us in Ref. [42]. That earlier model is theoretically equivalent to END/KSDFT, but it was implemented in an incipient form. However, the current END/KSDFT has been efficiently implemented in our new code *CSDYN* 1.0 (see Section 3) that can feasibly simulate larger systems.

2. Theory

Similar to SLEND, the END/KSDFT total wavefunction $|\Psi_{Total}\rangle$ is the product of a nuclear $|\Psi_N\rangle$ and electronic $|\Psi_e\rangle$ wavefunction: $|\Psi_{Total}\rangle = |\Psi_N\rangle|\Psi_e\rangle$. For N_N nuclei, $|\Psi_N\rangle$ is the product of $3N_N$ frozen, narrow-width, Gaussian wave packets:

$$|\Psi_N\rangle = |\mathbf{R},\mathbf{P}\rangle = \prod_{i=1}^{3N_N} \exp\left[-\left(\frac{X_i - R_i}{2\Delta R_i}\right)^2 + iP_i(X_i - R_i)\right] \tag{6}$$

with average positions R_i, average conjugate momenta P_i, and widths ΔR_i; R_i and P_i are the variational parameters of $|\Psi_N\rangle = |\mathbf{R},\mathbf{P}\rangle$. $|\Psi_N\rangle$ is treated under the TDVP in the limit of zero widths ΔR_i so that a nuclear classical dynamics in terms of the positions and momenta $\{R_i(t), P_i(t)\}$[1–3,11] is obtained [*cf.* Eq. (12)]. The electronic wavefunction $|\Psi_e\rangle$ is a single-determinantal state $|\mathbf{z},\mathbf{R}\rangle$ in the Thouless representation [10]. For $|\mathbf{z},\mathbf{R}\rangle$, one considers N_e occupied $\{\psi_h\}$ and $K - N_e$ virtual $\{\psi_p\}$ orthonormal molecular spin–orbitals (MSO) constructed with atomic basis set functions on the centers $\{R_i\}$ of the nuclear wave packets. Taking $|0\rangle = b_{N_e}^\dagger \ldots b_h^\dagger \ldots b_1^\dagger|\text{vac}\rangle$ as a reference, the Thouless single-determinantal state $|\Psi_e\rangle = |\mathbf{z},\mathbf{R}\rangle$ is [10]:

$$|\Psi_e\rangle = |\mathbf{z},\mathbf{R}\rangle = \det(\chi_h) = \exp\left(\sum_{p=N_e+1}^{K}\sum_{h=1}^{N_e} z_{ph} b_p^\dagger b_h\right)|0\rangle;$$
$$\chi_h = \psi_h + \sum_{p=N_e+1}^{K} z_{ph}\psi_p \tag{7}$$

where $\{\chi_h\}$ are the dynamical spin–orbitals (DSO) [1,10] in terms of the complex-valued Thouless parameters $\{z_{ph}\}$. Those parameters and the nuclear positions $\{R_i\}$ are the variational parameters of $|\Psi_e\rangle = |\mathbf{z},\mathbf{R}\rangle$. In Thouless' original formulation and in SLEND, Hartree–Fock MSO were used for $|\mathbf{z},\mathbf{R}\rangle$, but in END/KSDFT, they are substituted for KS MSO obtained from the time-independent KS equations [35,43]. The KS MSO and DSO are spin-unrestricted, thus $|\mathbf{z},\mathbf{R}\rangle$ can describe bond-breaking/forming processes. While the KS MSO are fully orthogonal, the DSO are non-orthogonal within spin blocks.

The advantages of employing a non-standard Thouless single-determinantal state in TDVP treatments are discussed in detail in Ref. [1–3,9] and summarized herein. Having a reference $|0\rangle$, the Thouless representation expresses all the single-determinantal states $|\mathbf{z},\mathbf{R}\rangle$ non-orthogonal to $|0\rangle$ in terms of the non-redundant parameters $\{z_{ph}\}$. Non-redundancy means that those parameters provide a one-to-one mapping between them and the non-equivalent states $|\mathbf{z},\mathbf{R}\rangle$. Therefore, the Thouless representation allows an unambiguous variational sampling of all the non-equivalent single-determinantal states non-orthogonal to $|0\rangle$. Such a representation also avoids the numerical instabilities associated with redundant parameterizations, like those in terms of the MSO atomic coefficients [1].

In SLEND, the Thouless single-determinantal state $|\mathbf{z},\mathbf{R}\rangle$ is an approximate electronic wavefunction of the actual system that provides an approximate electron density $\rho(\mathbf{r},t)$. In contrast, in END/KSDFT, $|\mathbf{z},\mathbf{R}\rangle$ acts as an auxiliary KS wavefunction that can provide the exact electron density $\rho(\mathbf{r},t)$ if $A_{xc}[\rho]$ (or $v_{xc}[\rho](\mathbf{r},t)$) is known exactly. The electron density $\rho(\mathbf{r},t)$ of the non-standard $|\mathbf{z},\mathbf{R}\rangle$ is

$$\rho(\mathbf{r};\mathbf{z},\mathbf{z}^*,\mathbf{R}) = \int ds\gamma_1(\mathbf{r}',s',\mathbf{r},s;\mathbf{z},\mathbf{z}^*,\mathbf{R})|_{\mathbf{r}'=\mathbf{r},s'=s} \tag{8}$$

with the one-electron reduced density matrix $\gamma_1(\mathbf{x}',\mathbf{x})$ [43,44] of $|\mathbf{z},\mathbf{R}\rangle$ [1]

$$\gamma_1(\mathbf{r}',s',\mathbf{r},s;\mathbf{z},\mathbf{z}^*,\mathbf{R}) = \sum_{i,j}^{K}\psi_i(\mathbf{r}',s';\mathbf{R})\gamma_{ij}^{(1)}(\mathbf{z},\mathbf{z}^*)\psi_j^*(\mathbf{r},s;\mathbf{R})$$
$$\gamma_{ij}^{(1)}(\mathbf{z},\mathbf{z}^*) = \frac{\langle\mathbf{z},\mathbf{R}\left|b_j^\dagger b_i\right|\mathbf{z},\mathbf{R}\rangle}{\langle\mathbf{z},\mathbf{R}|\mathbf{z},\mathbf{R}\rangle} = \begin{bmatrix}\mathbf{I}\\ \mathbf{z}\end{bmatrix}\left[\mathbf{I}+\mathbf{z}^\dagger\mathbf{z}\right]^{-1}\begin{bmatrix}\mathbf{I} & \mathbf{z}^\dagger\end{bmatrix} \tag{9}$$

where s and s' are spin variables, and $\mathbf{I} = (\delta_{ij}) \in \mathbb{R}^{N_e\times N_e}$ and $\mathbf{z} = (z_{ph}) \in \mathbb{C}^{(K-N_e)\times N_e}$ are the identity and Thouless parameter matrices, respectively.

The END/KSDFT quantum action $A[\mathbf{R},\mathbf{P},\rho] = A[\mathbf{R},\mathbf{P},\mathbf{z},\mathbf{z}^*] = \int_{t_1}^{t_2} dtL[\mathbf{R}(t),\mathbf{P}(t),\mathbf{z}(t),\mathbf{z}^*(t)]$ involves the quantum Lagrangian $L[\mathbf{R},\mathbf{P},\mathbf{z},\mathbf{z}^*]$ [*cf.* Eq. (1)] with $|\Psi_N\rangle$ evaluated in the limit of the zero widths ΔR_i, Eq. (6), and with the electronic energy, E_e, in the KSDFT form

$$\begin{aligned}L[\mathbf{R},\mathbf{P},\mathbf{z},\mathbf{z}^*] = &\sum_{j=1}^{3N_N}\left[P_j + \frac{i}{2}\left(\frac{\partial\ln S}{\partial R_j} - \frac{\partial\ln S}{\partial R_j'}\right)\right]\dot{R}_j\\ &+\frac{i}{2}\sum_{p,h}^{K-N_e,N_e}\left(\frac{\partial\ln S}{\partial z_{ph}}\dot{z}_{ph} - \frac{\partial\ln S}{\partial z_{ph}^*}\dot{z}_{ph}^*\right)\\ &-\sum_{i=1}^{N_N}\frac{\mathbf{P}_i^2}{2M_i} - \sum_{i=1,j>i}^{N_N}\frac{Z_iZ_j}{|\mathbf{R}_i-\mathbf{R}_j|} - E_e[\mathbf{R},\mathbf{z},\mathbf{z}^*]\end{aligned} \tag{10}$$

where the first and second terms in the last line are the classical nuclear kinetic and nuclear repulsive energies, respectively, and $S = \langle\mathbf{z}',\mathbf{R}'|\mathbf{z},\mathbf{R}\rangle$. The electronic energy E_e is

$$\begin{aligned}E_e[\mathbf{R},\mathbf{z},\mathbf{z}^*] = &\frac{\langle\mathbf{z},\mathbf{R}|\widehat{T}_e|\mathbf{z},\mathbf{R}\rangle}{\langle\mathbf{z},\mathbf{R}|\mathbf{z},\mathbf{R}\rangle} + \int d\mathbf{r}\rho(\mathbf{r};\mathbf{z},\mathbf{z}^*,\mathbf{R})v_{ext}(\mathbf{r};\mathbf{R})\\ &+\frac{1}{2}\int\int d\mathbf{r}d\mathbf{r}'\frac{\rho(\mathbf{r};\mathbf{z},\mathbf{z}^*,\mathbf{R})\rho(\mathbf{r}';\mathbf{z},\mathbf{z}^*,\mathbf{R})}{|\mathbf{r}-\mathbf{r}'|}\\ &+E_{xc}^{gs}[\rho(\mathbf{r};\mathbf{z},\mathbf{z}^*,\mathbf{R})]\end{aligned} \tag{11}$$

whose terms are the KS kinetic, external-potential, classical self-repulsion, and exchange–correlation energies, respectively [*cf.* Eq. (3)]. The external potential $v_{ext}(\mathbf{r};\mathbf{R}) = -\sum_{i=1}^{N_N} Z_i|\mathbf{r}-\mathbf{R}_i|^{-1}$ is caused by the moving nuclei. The adiabatic approximation is employed in Eq. (11) via $E_{xc}^{gs}[\rho]$ [*cf.* Eq. (5)]. The above END/KSDFT E_e is that of SLEND, but with the SLEND Hartree–Fock exchange term now substituted for a KSDFT exchange–correlation term.

Application of the standard TDVP to $A[\mathbf{R},\mathbf{P},\mathbf{z},\mathbf{z}^*]$ produces the END/KSDFT dynamical equations as a set of Euler–Lagrange equations for the variational parameters: $\{R_i(t), P_i(t), z_{ph}(t), z_{ph}^*(t)\}$ [1–3,9]:

$$\begin{bmatrix} i\mathbf{C} & \mathbf{0} & i\mathbf{C}_\mathbf{R} & \mathbf{0}\\ \mathbf{0} & -i\mathbf{C}^* & -i\mathbf{C}_\mathbf{R}^* & \mathbf{0}\\ i\mathbf{C}_\mathbf{R}^\dagger & -i\mathbf{C}_\mathbf{R}^T & \mathbf{C}_{\mathbf{RR}} & -\mathbf{I}\\ \mathbf{0} & \mathbf{0} & \mathbf{I} & \mathbf{0}\end{bmatrix}\begin{bmatrix}\frac{d\mathbf{z}}{dt}\\ \frac{d\mathbf{z}^*}{dt}\\ \frac{d\mathbf{R}}{dt}\\ \frac{d\mathbf{P}}{dt}\end{bmatrix} = \begin{bmatrix}\frac{\partial E_{Total}}{\partial\mathbf{z}^*}\\ \frac{\partial E_{Total}}{\partial\mathbf{z}}\\ \frac{\partial E_{Total}}{\partial\mathbf{R}}\\ \frac{\partial E_{Total}}{\partial\mathbf{P}}\end{bmatrix} \tag{12}$$

with total energy $E_{Total} = \sum_{i=1}^{N_N} \mathbf{P}_i^2/2M_i + \sum_{i=1,j>i}^{N_N} Z_i Z_j / |\mathbf{R}_i - \mathbf{R}_j|^{-1} + E_e$, and dynamic metric matrices:

$$(\mathbf{C}_{XY})_{ij,kl} = -2Im \frac{\partial^2 \ln S}{\partial X_{ik} \partial Y_{jl}}\bigg|_{\mathbf{R}'=\mathbf{R}}; \quad (\mathbf{C}_{X_{ik}})_{ph} = \frac{\partial^2 \ln S}{\partial z^*_{ph} \partial X_{ik}}\bigg|_{\mathbf{R}'=\mathbf{R}};$$
$$\mathbf{C}_{ph,qg} = \frac{\partial^2 \ln S}{\partial z^*_{ph} \partial z_{qg}}\bigg|_{\mathbf{R}'=\mathbf{R}} \tag{13}$$

The END/KSDFT dynamical equations are analogous to the SLEND ones, but with some of their terms in the KS form (KS MSO, exchange–correlation energy, *etc.*). Eqs. (12) and (13) are a quantum generalization of the classical Hamilton equations in symplectic notation [9,11] and express the coupled nuclear and electronic dynamics in terms of the pairs of conjugate variables $\{R_i(t), P_i(t)\}$ and $\left\{z_{ph}(t), z^*_{ph}(t)\right\}$, respectively. Like SLEND, the END/KSDFT equations contain the nonadiabatic coupling terms $\mathbf{C_R}$ and $\mathbf{C_{RR}}$, which are neglected in other Hartree–Fock- and TDDFT-based dynamics methods [1].

3. Numerical results and discussion

The END/KSDFT method is implemented into our program *CSDYN*1.0. That code was developed from the program *ENDyne* 2.8 (E. Deumens et al., *ENDyne* 2.8, Quantum Theory Project, University of Florida, Gainesville, FL, 1997), but it differs substantially from the originating code. Distinct features of *CSDYN*1.0 include: subroutines implementing END/KSDFT and its code parallelization, auxiliary codes to calculate various reactions properties (*e.g.* cross sections), and visualization tools to prepare animations of simulated reactions (*cf.* Fig. 3). *CSDYN* 1.0 features most of the standard, ground-state time-independent DFT functionals to be used in the adiabatic approximation.

The first series of numerical tests with END/KSDFT involve the simulations of normal mode vibrations of H_2, HF, H_2O, and NH_3 to determine dynamically their corresponding periods/wavenumbers. Those simulations were performed at the END/KSDFT/B3LYP/6-31G** level. In each simulation, the geometry distortion prompting the vibration was small enough to obtain harmonic oscillations (*cf.* Fig. 1); therefore, the END/KSDFT/B3LYP/6-31G** periods/wavenumbers can be checked for accuracy with those determined statically by standard normal mode analysis (NMA). In Table 1, END/KSDFT/B3LYP/6-31G** normal modes periods and wavenumbers are compared with their NMA/KSDFT/B3LYP/6-31G** counterparts and with NMA/HF/6-31G** and experimental wavenumbers. NMA/KSDFT/B3LYP/6-31G** results were calculated with the program GAMESS [45], while the NMA/HF/6-31G** and experimental data were taken from online databases of the National Institute of Standards and Technology; NMA/HF/6-31G** wavenumbers are equivalent to SLEND/6-31G** ones. All the END/KSDFT/B3LYP/6-31G** periods/wavenumbers agree very well with their NMA/KSDFT/B3LYP/6-31G** counterparts, which proves the correct END/KSDFT performance to simulate molecular vibrations. Notably, the END/KSDFT/B3LYP/6-31G** wavenumbers agree much better with the experimental ones than the NMA/HF/6-31G**(=SLEND/6-31G**) wavenumbers; this is expected since KSDFT predicts better vibrational wavenumbers than HF [46]. Fig. 1 illustrates some results from the simulation of the H_2O vibration in the B_2 asymmetric stretch mode. There, the H_2O total energy (E_{Total}), potential energy $\left(\sum_{i=1,j>i}^{N_N} Z_i Z_j / |\mathbf{R}_i - \mathbf{R}_j|^{-1} + E_e\right)$, O–H bond lengths, and total number of electrons are plotted *vs.* time. The sinusoidal patterns of the potential energy and bond lengths reveal harmonic oscillations, while the invariance of the total energy and total number of electrons demonstrate the END/KSDFT compliance with corresponding conservation laws.

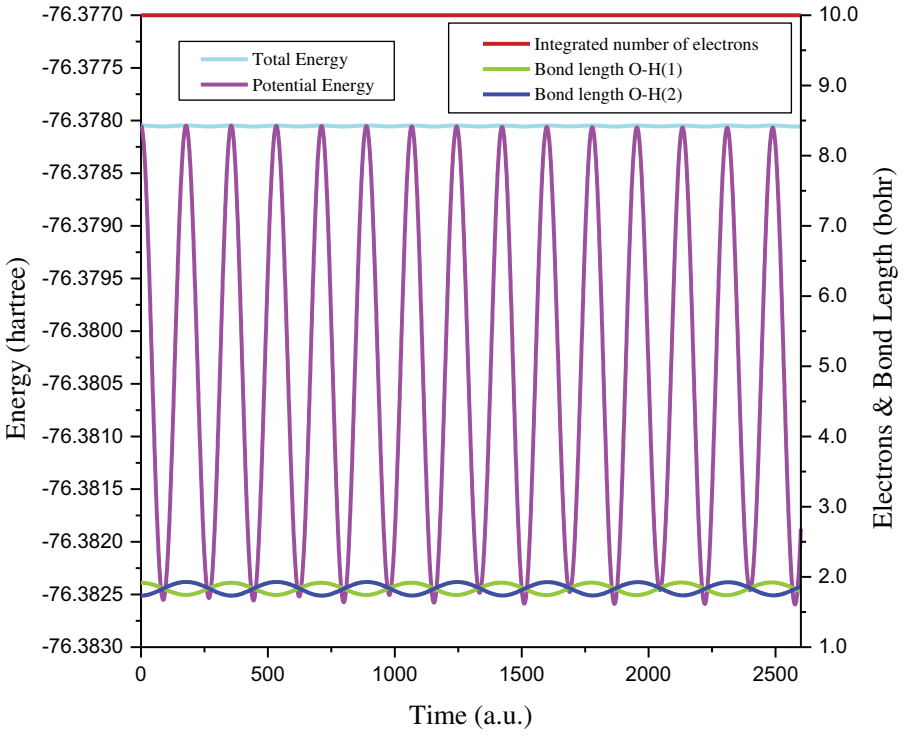

Fig. 1. Total and potential energies (left axis), O–H bond length (right axis), and total number of electrons (right axis) *vs.* time from the END/KSDFT/B3LYP/6-31G** simulation of H_2O in the B_2 asymmetric stretch mode.

Table 1
Normal mode periods (T) and wavenumbers ($\bar{\nu} = 1/Tc$) of representative molecules from END/KSDFT/B3LYP/6-31G** (dynamic) and normal mode analysis (NMA)/KSDFT/6-31G** [45] (static) calculations; wavenumbers from NMA/Hartree–Fock(HF)/6-31G** calculations and experiments (from the National Institute of Standard and Technology) are also listed.

Normal mode	T END/KSDFT ± 1 a.u. (fs)	T NMA/KSDFT a.u. (fs)	$\bar{\nu}$ END/KSDFT (cm^{-1})	$\bar{\nu}$ NMA/KSDFT (cm^{-1})	$\bar{\nu}$ NMA/HF (cm^{-1})	$\bar{\nu}$ Expt. (cm^{-1})
H_2–A_1 stretch	310 (7.5)	309 (7.5)	4448	4462	4635	4401.2
HF–A_1 stretch	339 (8.2)	338 (8.2)	4068	4084	4493	4138.4
H_2O–A_1 symmetric bend	832 (20.1)	832 (20.1)	1657	1665	1770	1595.0
H_2O–A_1 symmetric stretch	365 (8.8)	363 (8.8)	3778	3797	4148	3657.0
H_2O–B_2 asymmetric stretch	355 (8.6)	353 (8.5)	3885	3910	4265	3756.0
NH_3–A_1 symmetric bend	1272 (30.8)	1266 (30.6)	1084	1090	1142	950.0
NH_3–E asymmetric bend	815 (19.7)	814 (19.7)	1692	1693	1811	1627.0
NH_3–E symmetric bend	815 (19.7)	814 (19.7)	1692	1693	1811	1627.0
NH_3–A_1 symmetric stretch	399 (9.7)	399 (9.7)	3456	3458	3705	3337.0
NH_3–E symmetric stretch	386 (9.3)	385 (9.3)	3573	3586	3843	3444.0
NH_3–E asymmetric stretch	386 (9.3)	385 (9.3)	3573	3586	3843	3444.0

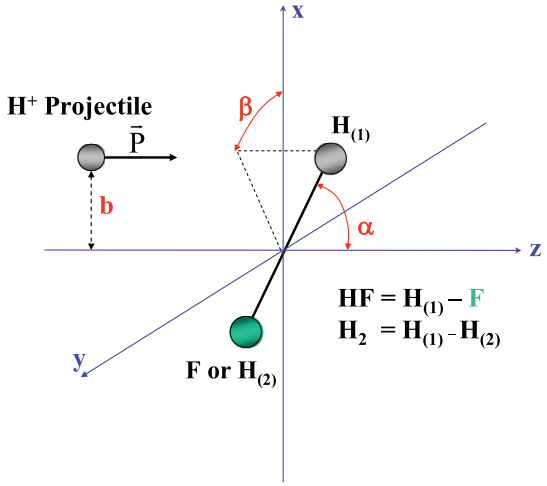

Fig. 2. $H^+ + H_2$ and $H^+ + HF$ reactants initial conditions. The balls represent the classical nuclei with projectile impact parameter b and molecule orientation $[\alpha,\beta]$.

The second series of numerical tests involves the simulations of the $H^+ + H_2$ and $H^+ + HF$ reactions at collision energy $E_{Lab} = 30$ eV, which were previously studied with SLEND [12,13,18]. Here, these reactions are simulated at the END/KSDFT/B3LYP/6-31G** and SLEND/6-31G** levels for the sake of comparison. For these simulations, the initial nuclear positions of the reactants are shown in Fig. 2. Nuclei originally in H_2 (HF) are labeled $H_{(1)}$ and $H_{(2)}$(F), respectively, and the incoming projectile H^+. Initially, the projectile is at position $\mathbf{R}_{H^+} = (b \geqslant 0.0, 0.0, -15.0$ a.u.), where b is the impact parameter, and with momentum $\mathbf{P}_{H^+} = (0.0, 0.0, P_z > 0)$ corresponding to $E_{Lab} = 30$ eV. The molecules' orientations $[\alpha,\beta]$ are determined by the angles: $0° \leqslant \alpha \leqslant 180°$ and $0° \leqslant \beta \leqslant 360°$ from the $H_{(1)}$ end. For H_2, two orientations are considered: [0°,0°] and [90°,0°], and for HF, one: [90°,0°]. Initially, the molecules are at rest, with the centers of mass at $\mathbf{R}^{c.m.}_{H_2/HF} = (0.0, 0.0, 0.0)$ and in the unrestricted KSDFT/B3LYP/6-31G** or HF/6-31G** ground state. All simulations are run for a total time of 1000 a.u. (24.2 fs).

The present simulations predict three processes: collision-induced molecule dissociation (D):

$$H^+_\bullet + H_2 \rightarrow H^q_\bullet + H^r + H^s;$$
$$H^+_\bullet + HF \rightarrow H^q_\bullet + H^r + F^s; \quad q + r + s = +1 \qquad (14)$$

where the bullet • marks the H nucleus originally in the H^+ projectile; hydrogen rearrangement (R):

$$H^+_\bullet + H_2 \rightarrow H^q + H_\bullet H^r; H^+_\bullet + HF \rightarrow H^q + H_\bullet F^r; \quad q + r = +1. \qquad (15)$$

and inelastic scattering (IS):

$$H^+_\bullet + H_2 \rightarrow H^q_\bullet + H^r_2; H^+_\bullet + HF \rightarrow H^q_\bullet + HF^r; \quad q + r = +1. \qquad (16)$$

Table 2 lists the processes' occurrences per initial molecule orientations and per projectile impact parameters. That table reveals that END/KSDFT/B3LYP/6-31G** and SLEND/6-31G** predict the same three processes in both systems over similar ranges of impact parameters. Figs. 3–5 provide interesting details of these simulations. Fig. 3 shows four snapshots of the END/KSDFT/B3LYP/6-31G** simulation of $H^+ + HF$ from $[90°,0°]/b = 1.9$ a.u. that leads to an R process. There, the small balls represent the nuclei (green ball = F, gray balls = H) and the colored clouds, electron density isosurfaces increasing in value through the sequence: purple, blue, yellow, and red. Those snapshots depict four stages of the R process: $H^+ + H_{(1)}F \rightarrow H^+_{(1)} + HF$. Figs. 4 and 5 compare the nuclear relative distances *vs.* time of END/KSDFT/B3LYP/6-31G** and SLEND/6-31G** simulations of $H^+ + H_2$ from $[90°, 0°]/b = 0.9$ a.u. (R, Fig. 4) and of $H^+ + HF$ from $[90°, 0°]/b = 1.9$ a.u. (R, Fig. 5). Figs. 4 and 5 reveal some differences between the END/KSDFT/B3LYP/6-31G** and SLEND/6-31G** dynamics (*e.g.*. trajectory and rearrangement details, post-collision vibrational motions, *etc.*) that are likely caused by the different levels of electron correlation in the compared methods.

Table 2
Reactive processes in $H^+ + H_2$ and $H^+ + HF$ at $E_{Lab} = 30$ eV, per initial molecule orientations $[\alpha,\beta]$ and per projectile impact parameter b, from END/KSDFT/B3LYP/ 6-31G** and SLEND/6-31G** simulations. D = collision-induced dissociation (Eq. (14)), R = hydrogen rearrangement (Eq. (15)), IS = inelastic scattering (Eq. (16)).

b (a.u.)	$H^+ + H_2$				$H^+ + HF$	
	[90°,0°] Orientation		[0°,0°] Orientation		[90°,0°] Orientation	
	END/KSDFT	END	END/KSDFT	END	END/KSDFT	END
0.0	D	D	R	R	IS	IS
0.1	D	D	D	R	IS	IS
0.2	D	D	R	R	IS	IS
0.3–0.4	D	D	D	D	IS	IS
0.5	D	D	D	IS	IS	IS
0.6	R	D	IS	IS	D	IS
0.7–0.9	R	R	IS	IS	D	D
1.0	D	R	IS	IS	R	D
1.1	D	R	IS	IS	D	R
1.2–1.3	D	D	IS	IS	D	R
1.4	IS	IS	IS	IS	D	D
1.5	IS	IS	IS	IS	R	D
1.6–2.0	IS	IS	IS	IS	R	R
2.1	IS	IS	IS	IS	D	R
2.2–2.4	IS	IS	IS	IS	D	D
2.5	IS	IS	IS	IS	IS	D
⩾2.6	IS	IS	IS	IS	IS	IS

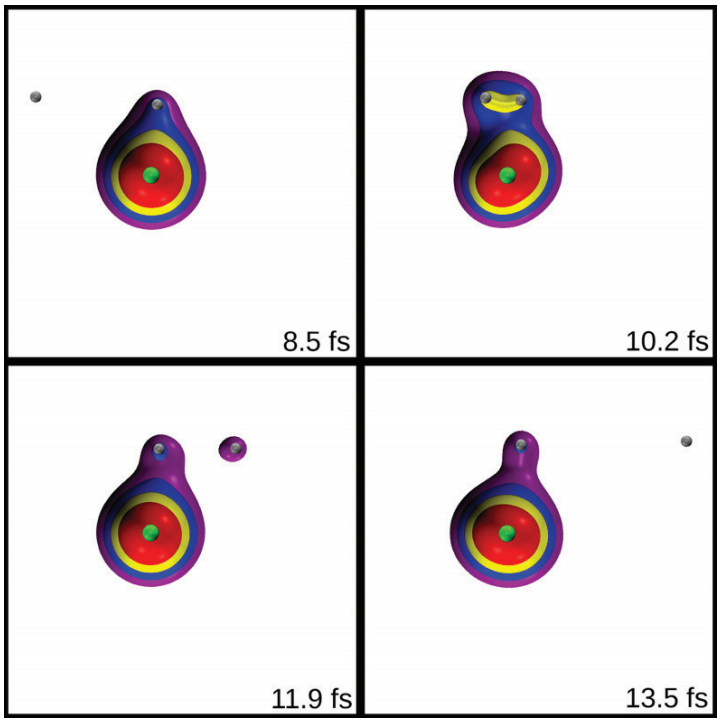

Fig. 3. Four snapshots of the END/KSDFT/B3LYP/6-31G** simulation of $H^+ + HF$ at E_{Lab} = 30 eV from molecule orientation [90°,0°] and impact parameter b = 1.9 a.u. Snapshot times shown in femtoseconds (fs). The balls represent the nuclei (green ball = F, gray balls = H) and the colored clouds, electron density isosurfaces increasing in value through the sequence: purple, blue, yellow, and red. The snapshots show a hydrogen rearrangement reaction [R, Eq. (15)]. Snapshots prepared with VMD [47] and Tachyon [48] software. (For interpretation of the references to colour in this figure legend, the reader is referred to the web version of this Letter.)

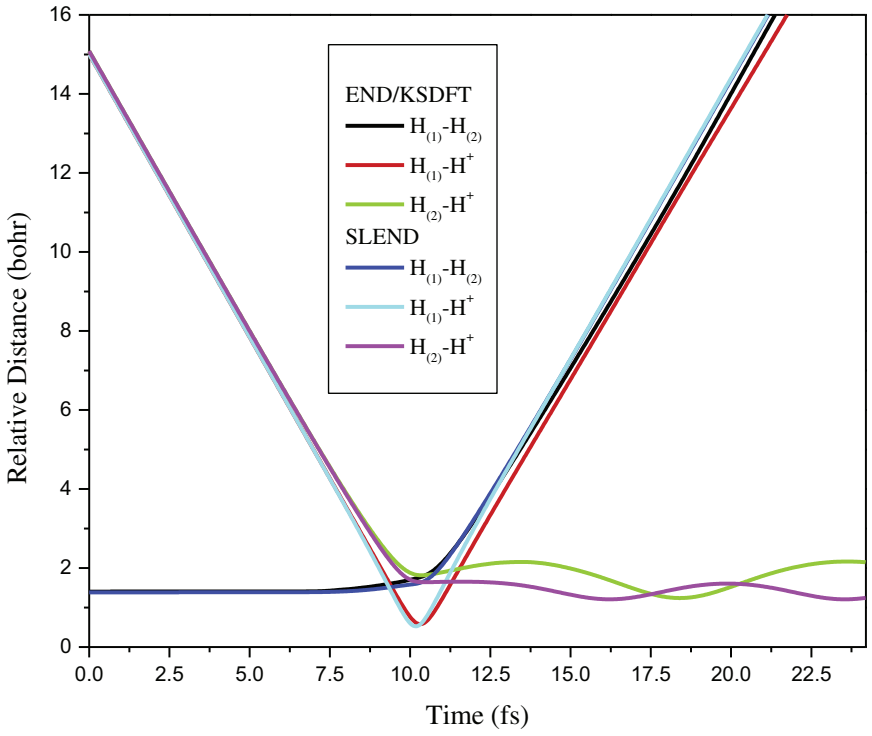

Fig. 4. Nuclear relative distances *vs.* time of the END/KSDFT/B3LYP/6-31G** and END/6-31G** simulations of $H^+ + H_2$ at E_{Lab} = 30 eV from the molecule orientation [90°, 0°] and impact parameter b = 0.9 a.u. Both methods predict rearrangement [R, Eq. (15)].

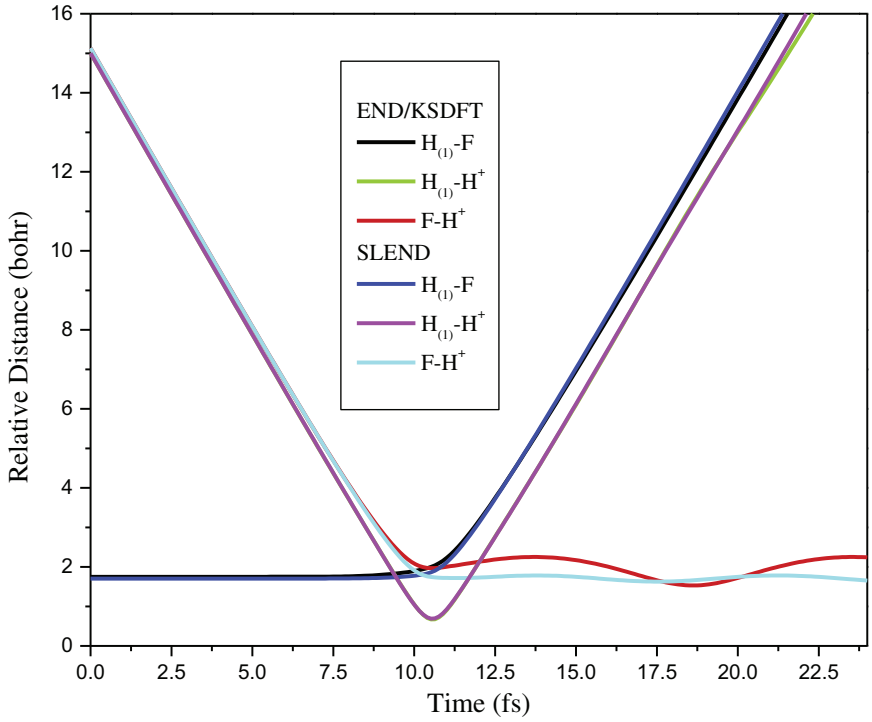

Fig. 5. Nuclear relative distances *vs.* time of END/KSDFT/B3LYP/6-31G** and END/6-31G** simulations of $H^+ + HF$ at E_{Lab} = 30 eV from molecule orientation [90°,0°] and impact parameter b = 1.9 a.u. Both methods predict hydrogen rearrangement [R, Eq. (15)].

4. Summary and future work

The END/KSDFT method that incorporates TDKSDFT [31–34] capabilities into the SLEND [1–3] framework has been presented. Like SLEND, END/KSDFT adopts a classical-mechanics description for the nuclei and a Thouless single-determinantal representation [10] for the electrons. However, the electronic description is now reformulated in a KSDFT fashion that provides electron correlation effects absent in SLEND. The END/KSDFT dynamical equations are obtained by applying the TDVP [9] to the END/KSDFT quantum action with the adiabatic approximation [32–34] employed in its exchange–correlation part. Simulations of H_2, HF, H_2O, and NH_3 normal mode vibrations and of the $H^+ + H_2$ and $H^+ + HF$ reactions at E_{Lab} = 30 eV illustrate the correctness of END/KSDFT to describe those systems. Present efforts concentrate on applying END/KSDFT to more complex reactions and on developing the additional theoretical aspects of END/KSDFT discussed in the introduction.

Acknowledgments

The authors thank Mr. Prakash Varma for running some DFT tests and the Texas Tech University High Performance Computer Center for computer time. This material is based upon work partially supported by the National Science Foundation under Grant CHE-0645374 (CAREER) and by the Robert A. Welch Foundation under Grant D-1539. Acknowledgement is also made to the donors of The American Chemical Society Petroleum Research fund for partial support of this research.

References

[1] E. Deumens, A. Diz, R. Longo, Y. Öhrn, Rev. Mod. Phys. 66 (1994) 917.
[2] E. Deumens, Y. Öhrn, J. Chem. Soc., Faraday Trans. 93 (1997) 919.
[3] E. Deumens, Y. Öhrn, J. Phys. Chem. A 105 (2001) 2660.
[4] I.S.Y. Wang, M. Karplus, J. Am. Chem. Soc. 95 (1973) 8160.
[5] C. Leforestier, J. Chem. Phys. 68 (1978) 4406.
[6] R. Car, M. Parrinello, Phys. Rev. Lett. 55 (1985) 2471.
[7] K. Bolton, W.L. Hase, G.H. Peslherbe, in: D.L. Thompson (Ed.), Multidimensional Molecular Dynamics Methods, World Scientific Publishing, London, 1998, p. 143.
[8] L. Sun, W.L. Hase, in: K.B. Lipkowitz, R. Larter, T.R. Cundari (Eds.), Reviews in Computational Chemistry, vol. 19, Wiley, New York, NY, 2003, p. 79.
[9] P. Kramer, M. Saraceno, Geometry of the Time-Dependent Variational Principle in Quantum Mechanics, Springer-Verlag, New York, 1981.
[10] D.J. Thouless, Nucl. Phys. 21 (1960) 225.
[11] H. Goldstein, Classical Mechanics, Addison-Wesley, Reading, MA, 1980.
[12] J.A. Morales, A.C. Diz, E. Deumens, Y. Öhrn, Chem. Phys. Lett. 233 (1995) 392.
[13] J.A. Morales, A. Diz, E. Deumens, Y. Öhrn, J. Chem. Phys. 103 (1995) 9968.
[14] D. Jacquemin, J.A. Morales, E. Deumens, Y. Öhrn, J. Chem. Phys. 107 (1997) 6146.
[15] M. Hedström, J.A. Morales, E. Deumens, Y. Öhrn, Chem. Phys. Lett. 279 (1997) 241.
[16] S.A. Malinovskaya, R. Cabrera-Trujillo, J.R. Sabin, E. Deumens, Y. Öhrn, J. Chem. Phys. 117 (2002) 1103.
[17] J.A. Morales, B. Maiti, Y. Yan, K. Tsereteli, J. Laraque, S. Addepalli, C. Myers, Chem. Phys. Lett. 414 (2005) 405.
[18] B. Maiti, R. Sadeghi, A. Austin, J.A. Morales, Chem. Phys. 340 (2007) 105.
[19] B. Maiti, P.M. McLaurin, R. Sadeghi, S.A. Perera, J.A. Morales, Int. J. Quant. Chem. 109 (2009) 3026.
[20] R. Cabrera-Trujillo, Y. Öhrn, E. Deumens, J.R. Sabin, J. Phys. Chem. A 108 (2004) 8935.
[21] M. Coutinho-Neto, E. Deumens, Y. Öhrn, Int. J. Quant. Chem. 77 (2000) 301.
[22] M. Coutinho-Neto, E. Deumens, Y. Öhrn, J. Chem. Phys. 116 (2002) 2794.
[23] H. Nakai, Int. J. Quant. Chem. 86 (2002) 511.
[24] A. Chakraborty, M.V. Pak, S. Hammes-Schiffer, Phys. Rev. Lett. 101 (2008) 153001.
[25] J.A. Morales, E. Deumens, Y. Öhrn, J. Math. Phys. 40 (1999) 766.
[26] J.R. Klauder, B.S. Skagerstam, Coherent States, Application in Physics and Mathematical Physics, World Scientific, Singapore, 1985.
[27] J.A. Morales, J. Phys. Chem. A 113 (2009) 6004.
[28] R. McWeeney, Methods of Molecular Quantum Mechanics, Academic Press, London, 1992.
[29] E. Deumens, Y. Öhrn, B. Weiner, J. Math. Phys. 32 (1991) 1166.
[30] R.J. Bartlett, M. Musial, Rev. Mod. Phys. 79 (2007) 291.
[31] E. Runge, E.K.U. Gross, Phys. Rev. Lett. 52 (1984) 997.
[32] E.K.U. Gross, W. Kohn, Adv. Quant. Chem. 21 (1990) 255.
[33] E.K.U. Gross, J.F. Dobson, M. Petersilka, in: R.F. Nalewajaki (Ed.), Topics in Current Chemistry, vol. 181, Springer, Berlin, 1996, p. 81.

[34] M.A.L. Marques, E.K.U. Gross, Ann. Rev. Phys. Chem. 55 (2004) 427.
[35] W. Kohn, L.J. Sham, Phys. Rev. 140 (1965) A1133.
[36] J. Theilhaber, Phys. Rev. B 46 (1992) 12990.
[37] R. van Leeuwen, Phys. Rev. Lett. 80 (1998) 1280.
[38] R. Van Leeuwen, Int. J. Mod. Phys. A 15 (2001) 1969.
[39] A.K. Rajagopal, Phys. Rev. A 54 (1996) 3916.
[40] S. Mukamel, Phys. Rev. A 71 (2005) 024503.
[41] G. Vignale, Phys. Rev. A 77 (2009) 062511.
[42] K. Tsereteli, Y. Yan, J.A. Morales, Chem. Phys. Lett. 420 (2006) 54.
[43] R.G. Parr, W. Yang, Density-Functional Theory of Atoms and Molecules, Oxford University Press, New York, 1989.
[44] A. Szabo, N.S. Ostlund, Modern Quantum Chemistry, Dover Publications, Inc., Mineola, NY, 1989.
[45] M.W. Schmidt et al., J. Comput. Chem. 14 (1993) 1347.
[46] I.N. Levine, Quantum Chemistry, Prentice-Hall, Upper Saddle River, NJ, 2008.
[47] W. Humphrey, A. Dalke, K. Shulten, J. Mol. Graphics 14 (1996) 33.
[48] J. Stone, An Efficient Library for Parallel Ray Tracing and Animation, Master Thesis, University of Missouri-Rolla, 1998.